



Structural and Conformational Analysis of 1-Butyl-3-methylimidazolium Nitrate

Dean H. Johnston¹ · Mallory Gasbarre¹ · Carolanne E. Norris¹

Received: 29 April 2021 / Accepted: 3 August 2021

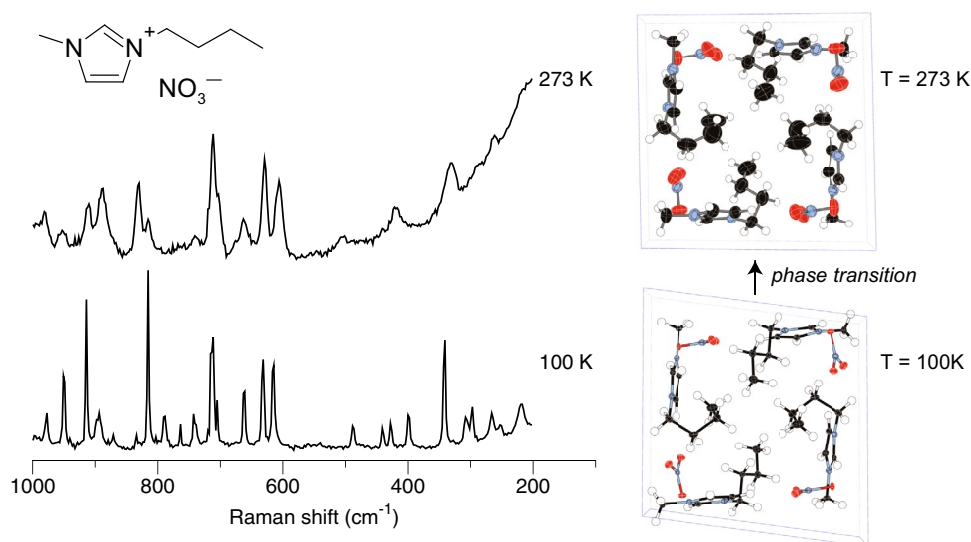
© The Author(s), under exclusive licence to Springer Science+Business Media, LLC, part of Springer Nature 2021

Abstract

The crystal structures of two polymorphic forms of 1-butyl-3-methylimidazolium nitrate are reported. The form observed at 100 K and 200 K (**Ia** and **Ib**) crystallizes in the $P\bar{1}$ space group and contains two independent imidazolium cations and nitrate anions. At 100 K the butyl chain of one cation adopts a TT (*trans-trans*) conformation and the other cation adopts a G'G' (*gauche-gauche*) conformation. At 200 K, the G'G' chain is disordered with about twelve percent of the GT conformation present. A different polymorph (Form **II**, also crystallizing in the $P\bar{1}$ space group with two independent ion pairs) is present at 273 K displaying significant disorder in the butyl chains with a mixture of G'T, G'G', and GT conformers. Raman spectra were collected on samples between 100 and 350 K and show changes in band frequencies and intensities consistent with conversion between different butyl chain conformations. Hydrogen bond interactions are present between cation C-H's and oxygen atoms of the nitrate ions, with significant lengthening observed for three of the six close contacts (and formation of one new contact) upon conversion to the higher-temperature form. The structural details revealed in this study shed light on the intermolecular forces and the conformational changes that accompany phase changes in 1-butyl-3-methylimidazolium nitrate.

Graphic Abstract

X-ray diffraction and Raman spectroscopy of the ionic liquid 1-butyl-3-methylimidazolium nitrate at temperatures from 100 to 300 K show evidence of two different polymorphs and significant temperature-dependent conformational changes.



Keywords Ionic liquids · Raman spectroscopy · Conformational isomerism · Crystal polymorphism

Extended author information available on the last page of the article

Introduction

Ionic liquids have widespread applications in chemical synthesis, catalysis and electrochemistry due to their high thermal and electrochemical stability, large liquid range, low vapor pressure and ability to solubilize a variety of materials [1–3]. A major challenge in the study and application of ionic liquids is understanding their structures and how intermolecular forces determine their properties. The wide range of molecular interactions present in ionic liquids [4], from weak dispersion forces to strong Coulombic interactions and hydrogen bonds, further complicates this analysis.

Crystallography is a powerful tool for analyzing the structures of ionic liquids and for determining the presence and influence of different intermolecular forces [5, 6]. Approaches such as in situ crystallization [7] and high-pressure studies [8] have helped overcome the challenges in isolating single-crystal samples of ionic liquids. The structures of at least eighteen metal-free salts of the 1-butyl-3-methylimidazolium ($[C_4mim]^+$) cation are known, including fluoride [9, 10], chloride [11–14], bromide [11, 15, 16], hexafluorophosphate [7, 17, 18], several tetraphenyl or tetraalkylborates [19–23], tosylate [16], bis(trifluoromethanesulfonyl)imide [24], triflate [7] and others [25–27]. Both the chloride and hexafluorophosphate salts exhibit polymorphism [11, 18, 28, 29] leading to extensive studies of the origins and the influence of intermolecular interactions on the nature of the observed polymorphic forms.

While the $[C_4mim][NO_3]$ ionic liquid has not been structurally characterized by single-crystal X-ray methods, several studies have examined the properties of the 1-alkyl-3-methylimidazolium nitrate ($[C_nmim][NO_3]$) family of ionic liquids. Molecular dynamics simulations have been used to model the phase transitions of the $[C_nmim][NO_3]$ ($n = 4–12$) ionic liquids, identifying the formation of a metastable state prior to the melting of the ionic liquid [30]. Strechan and coworkers published a detailed analysis of the thermal properties of 1-butyl-3-methylimidazolium nitrate [31], demonstrating the existence of four different crystal forms from the three solid-phase phase transitions observed between 278 and 310 K. They speculate that the phase transitions in $[C_4mim][NO_3]$ result from an order-disorder transformation of the nitrate ions, but conformational rearrangements of the butyl sidechain of the cation likely also play a significant role [32]. Abe et al. [33] used simultaneous differential scanning calorimetry (DSC) and powder X-ray diffraction measurements to identify two of the crystal phases that form during the heating of cold-crystallized neat $[C_4mim][NO_3]$, but only reported unit cell parameters and possible space groups.

Raman spectroscopy has been an important tool for the identification of polymorphic forms of $[C_4mim]^+$ salts, taking advantage of distinctive bands observed for the vibrations of the cation. In 2003, Hamaguchi et al. [15, 28] identified Raman bands unique to specific polymorphs and crystal forms of the chloride and bromide salts assignable to conformational isomers of the 1-butyl-3-methylimidazolium cation. This work was quickly followed by Raman spectroscopy and *ab initio* calculations of the $[C_4mim][PF_6]$ ionic liquid [34, 35]. Additional studies have examined the vibrational spectroscopy and conformational isomerism in the tetrafluoroborate salt [36, 37]. More recent studies have combined detailed computational work with spectroscopic, thermal and X-ray characterization [18, 29, 32]. All of this work has been summarized in several comprehensive reviews [38–41] and demonstrates how valuable Raman spectroscopy can be in identifying conformers present in both crystalline and liquid samples of alkyimidazolium-based ionic liquids, including a recent analysis of water confinement in $[C_4mim][NO_3]$ [42].

The torsion angles of interest correspond to $N-C_\alpha-C_\beta-C_\gamma$ and $C_\alpha-C_\beta-C_\gamma-C_\delta$ (see Fig. 1) for the butyl groups of each imidazolium cation. The lowest-energy conformations are *trans* (T, 180°) and *gauche* (G, 60°), with the added possibility of positive or negative torsion angles for the *gauche* configuration, annotated here as G and G' [18]. These possibilities generate at least nine conformers, some of which can be distinguished by Raman spectroscopy [41] and all of which have been extensively modeled via computational methods [18, 32].

In this study we report the first single crystal X-ray structures of two crystal forms of 1-butyl-3-methylimidazolium nitrate including an analysis of the hydrogen bonding network formed in the solid state. We also present Raman data collected at temperatures ranging from 100 to 350 K, spanning both the solid and liquid forms, and correlate the spectral features with the conformers identified from the crystallographic data. Through these data we confirm the existence of two different polymorphs of $[C_4mim][NO_3]$, providing insight into the importance of hydrogen bonding interactions, the relative stability of the two structures, and the transition from solid to liquid.

Experimental

Synthesis and Crystallization

All reagents, 1-methylimidazole (ACROS Organics, 99%), 1-bromobutane (ACROS Organics, 99%) and silver nitrate (Fisher ACS) were purchased from Fisher Scientific and used as received.

The 1-butyl-3-methylimidazolium bromide and 1-butyl-3-methylimidazolium nitrate were prepared using a modified version of the procedure described by Gruzdev et al. [43] and outlined in Scheme 1. A quantity of 10.17 g of 1-methylimidazole was placed in a 150-mL round bottom flask to which was added 16.69 g of 1-bromobutane. The flask was capped and the mixture was allowed to stir at room temperature for 1 week producing a viscous honey-colored liquid. The product was placed under vacuum to remove any potentially unreacted 1-bromobutane.

The 1-butyl-3-methylimidazolium bromide obtained in the first step was used without further purification and 16.67 g was placed in an Erlenmeyer flask along with 30 mL of deionized water. A sample of 12.70 g of silver nitrate was dissolved in 20 mL of deionized water and added dropwise to the 1-butyl-3-methylimidazolium bromide solution. The solution was stirred in the dark for 1 day after which the silver bromide precipitate was filtered off and the water was removed using a rotary evaporator. The 1-butyl-3-methylimidazolium nitrate product was obtained as a light-yellow viscous oil. ^1H NMR (300 MHz DMSO): δ = 0.84 (t, 3H, CH_2CH_3 , $J_{\text{HH}} = 7.35$ Hz), 1.22 (m, 2H, CH_2CH_3 , $J_{\text{HH}} = 7.62$ Hz), 1.75 (m, 2H, $\text{CH}_2\text{CH}_2\text{CH}_3$, $J_{\text{HH}} = 7.26$ Hz), 3.85 (s, 3H, NCH_3), 4.15 (t, 2H, $J_{\text{HH}} = 7.26$ Hz), 7.62 [s, 1H, H5 (Im)], 7.70 [s, 1H, H4 (Im)], 9.00 [s, 1H, H2 (Im)]. Storage of the product in an air-tight Schlenk flask for several months resulted in formation of a solid crystalline product.

X-Ray Diffraction: Sample Preparation, Data Collection, and Data Processing

Due to the tendency for samples to melt during inspection and mounting, crystals were prepared on a cooled microscope slide using a μCHILL [44] apparatus connected to an Oxford DTC Desktop Cooler.

Diffraction data was collected using a Bruker AXS SMART APEX II CCD diffractometer equipped with Mo $\text{K}\alpha$ sealed-tube radiation ($\lambda = 0.71073$ Å) and an Oxford Cryostream 700 low temperature device. Data were collected using a wide frame (2.0°) strategy (APEX3 [45]) for all structures.

Data sets were collected at three different temperatures, 100 K, 200 K and 273 K. Multiple samples were analyzed at 200 K, ensuring that the same unit cell and structural parameters were obtained for samples that were flash-cooled to 200 K versus samples that were initially analyzed at higher temperature and then cooled to 200 K. Several attempts to

collect data at 283 K indexed to the same unit cell found at 273 K, but did not give data of sufficient quality to produce a structure solution.

Cell refinement and data integration were performed using SAINT [45] with a wide-frame algorithm and SADABS [45] was used for absorption correction.

X-Ray Diffraction: Structure Solution, Refinement, and Treatment of Disorder

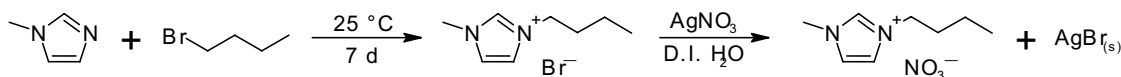
Structures were solved using SHELXT [46] and refined using SHELXL [47] using the Olex2 GUI [48]. All hydrogen atoms were located in the difference map and placed in idealized positions using a riding model, with $U_{\text{iso}}(\text{H}) = 1.2U_{\text{eq}}(\text{C})$ (ring or CH_2) or $U_{\text{iso}}(\text{H}) = 1.5U_{\text{eq}}(\text{C})$ (CH_3). Potential C–H \cdots O contacts were identified using the HTAB command in Olex2 [48] with a minimum angle of 120° and maximum donor-acceptor distance of 3.34 Å. Molecular graphics were prepared using CrystalMaker [49].

Structure Ia The structure at 100 K crystallized in the $P\bar{1}$ space group and was fully ordered.

Structure Ib The structure at 200 K crystallized in the $P\bar{1}$ space group and showed disorder in the C12, C13 and C14 atoms of the butyl chain of one $[\text{C}_4\text{mim}]^+$ cation [0.876(4):0.124(4)]. All 1–2 and 1–3 distances in the butyl chains were restrained to be the same (SADI) for the two cations using default tolerances. Rigid bond restraints (RIGU) were applied to all carbon atoms of the disordered butyl chain. The hydrogen atoms on the methyl group of one cation (C16) were modeled as rotationally disordered (AFIX 123), resulting in a refined occupancy of [0.61(2):0.39(2)] for the two positions.

Structure II The structure at 273 K also crystallized in the $P\bar{1}$ space group and showed disorder for the butyl chains of both imidazolium cations. The disorder of the two chains was originally modeled independently, but after refinement showed identical occupancies for the major component of both chains, a single free variable was assigned to model both disordered chains, refining to [0.569(6):0.431(6)]. All 1–2 and 1–3 distances in the butyl chains were restrained to be the same (SADI) for the two cations using default tolerances. Rigid bond restraints (RIGU) were applied to all carbon atoms of the disordered butyl chains.

Crystal data, data collection, and structure refinement details are summarized in Table 1. Crystallographic data has been deposited with the Cambridge Crystallographic Data Centre as CCDC 2010507 (**Ia**) CCDC 2010508 (**Ib**)



Scheme 1 Preparation of 1-butyl-3-methylimidazolium nitrate

Table 1 Summary of crystallographic data collection and refinement

	(Ia)	(Ib)	(II)
Chemical formula	C ₈ H ₁₅ N ₂ ·NO ₃	C ₈ H ₁₅ N ₂ ·NO ₃	C ₈ H ₁₅ N ₂ ·NO ₃
Temperature (K)	100	200	273
Space group	<i>P</i> $\bar{1}$	<i>P</i> $\bar{1}$	<i>P</i> $\bar{1}$
a (Å)	8.0411 (5)	8.1074 (7)	7.9872 (7)
b (Å)	11.3114 (7)	11.4318 (10)	11.7615 (10)
c (Å)	11.5416 (7)	11.5759 (10)	11.8119 (10)
α (°)	82.364 (1)	81.866 (2)	88.523 (2)
β (°)	84.123 (1)	84.952 (2)	80.462 (2)
γ (°)	86.510 (1)	86.620 (2)	87.778 (2)
V (Å ³)	1033.81 (11)	1056.79 (16)	1093.25 (16)
Z	4	4	4
μ (mm ⁻¹)	0.10	0.10	0.09
Crystal size (mm)	0.46 × 0.35 × 0.23	0.56 × 0.52 × 0.50	0.56 × 0.52 × 0.50
<i>T</i> _{min} , <i>T</i> _{max}	0.725, 0.746	0.594, 0.745	0.705, 0.745
Measured reflections	27633	22995	25189
Unique reflections	4756	3746	3869
Obs. reflections [<i>I</i> > 2 σ (<i>I</i>)]	3917	3035	3028
Number of parameters	257	286	314
Number of restraints	0	48	126
<i>R</i> _{int}	0.037	0.038	0.026
GOF	1.03	1.07	1.03
<i>R</i> [<i>I</i> > 2 σ (<i>I</i>)]	0.035	0.039	0.055
<i>wR</i>	0.085	0.104	0.166
Resid. density (e Å ⁻³)	0.23, -0.23	0.20, -0.19	0.21, -0.17

and CCDC 2010509 (II). These data can be obtained free of charge via <https://www.ccdc.cam.ac.uk/structures/> (or from the Cambridge Crystallographic Data Centre, 12 Union Road, Cambridge CB2 1EZ, UK; fax: (+44) 1223-336-033; or deposit@ccdc.ca.ac.uk).

Conformational Analysis and Database Searching

A detailed analysis of the imidazolium butyl chain conformation within **Ia**, **Ib**, **II**, and related structures was completed. The torsion angle notation described by Saoane, et al. [18] is used here (see Fig. 1): S (*syn*, -30 to +30°), G (*gauche*, +30 to +90°), G' (*gauche'*, -30 to -90°), E (*eclipsed*, +90 to +150°), E' (*eclipsed'*, -90 to -150°), and T (*trans*, -150 to +150°).

The Cambridge Structural Database [50] was searched using a combination of conventional search queries and SMARTS [51] substructure searches executed using the CSD Python API. The flexibility of the SMARTS query provided comprehensive search results since the placement and representation of the bonds in the imidazolium ring can vary between entries. A Python script was used to analyze butyl chain conformations including conformations and occupancies of disordered chains. The script and documentation is available at <https://gitlab.com/djohnston66/bmim-analysis>.

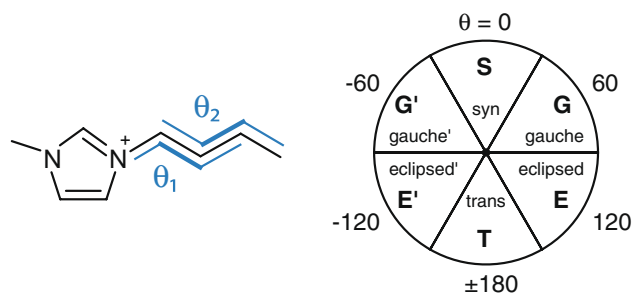


Fig. 1 Illustration of the imidazolium butyl chain torsion angles, θ_1 and θ_2 , and the corresponding conformational labels (Color figure online)

Graphs were generated using DataGraph, Version 4.7. Copyright ©2021 Visual Data Tools, Inc., Chapel Hill, NC, USA. Available at: <https://www.visualdatatools.com/>

Raman Spectroscopy

Dispersive Raman spectra were collected using a Jobin-Yvon LabRam 800HR at an excitation wavelength of 532.15 nm generated by a frequency-doubled Nd:YAG laser. Spectra were collected with a 950 grooves/mm

grating and calibrated using a silicon reference. Samples were loaded into a Linkam BCS196 low temperature stage and Raman spectra were collected at temperatures ranging from 100 to 350 K.

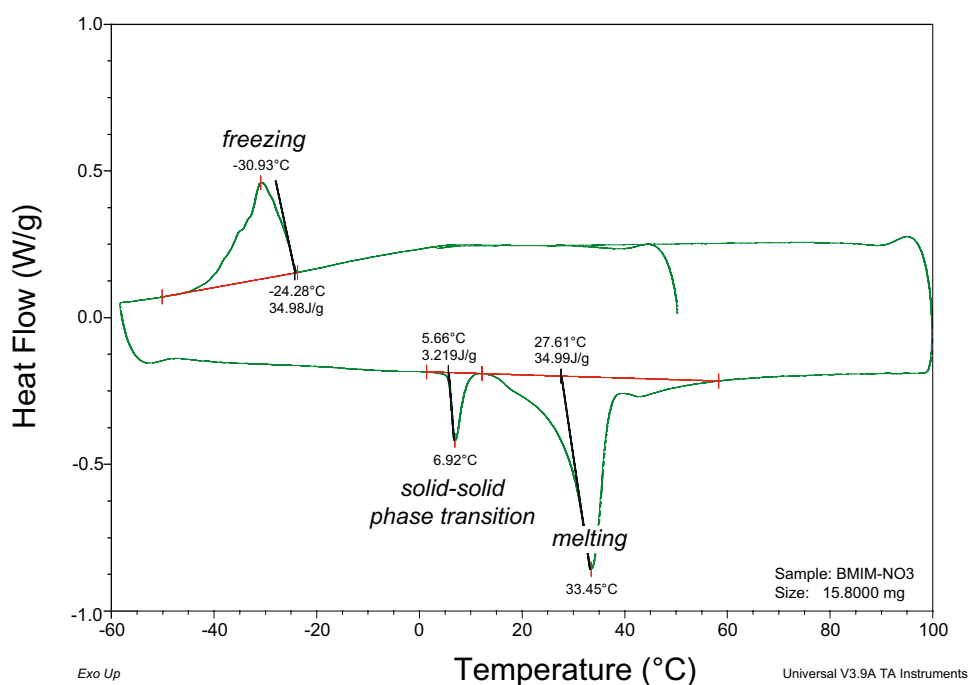
Thermal Analysis

Differential scanning calorimetry (DSC) measurements were conducted using a TA Instruments 2010 DSC. A 15.800 mg sample of 1-butyl-3-methylimidazoium nitrate was analyzed with heating rate of 10 °C/min and the resulting curve is shown in Fig. 2. The curve displays a broad melting curve between 15 and 40 °C that likely represents multiple phase transitions. [31] A smaller endothermic transition occurs around 5 °C, presumably corresponding to the conversion from Form I to Form II. The results are qualitatively in agreement with previous work [31, 43] but show differences due to differing techniques ([31]) or the absence of substantial water content ([43]).

Computational Analysis

Density functional calculations were run using Spartan' 18 [52] with the B3LYP functional and the 6-311+G(2df, 2p) basis set using the refined crystallographic atomic coordinates of each unique $[\text{C}_4\text{mim}]^+$ ion conformer as a starting point. Approximate Raman intensities were calculated assuming an excitation wavelength of 532 cm^{-1} and a temperature of 298 K.

Fig. 2 Differential scanning calorimetry (DSC) curve displaying phase transitions for a sample of 1-butyl-3-methylimidazoium nitrate. Heating rate = 10 °C/min (Color figure online)



Results and Discussion

X-Ray Crystal Structures and Hydrogen Bonding

This study represents the first full structural characterization of the $[\text{C}_4\text{mim}][\text{NO}_3]$ ionic liquid. Full datasets were collected at temperatures of 100 K, 200 K and 273 K. The space group for all three structures was $P\bar{1}$. Displacement ellipsoid diagrams showing the atom numbering schemes for all three structures are shown in Fig. 3. The asymmetric unit contains two independent copies of the $[\text{C}_4\text{mim}][\text{NO}_3]$ unit. The structures at 100 K and 200 K (**Ia** and **Ib**, respectively) were found to be very similar with relatively small changes in the unit cell parameters ($\Delta a/\sigma = +111$, $\Delta b/\sigma = +142$, $\Delta c/\sigma = +40$) and disorder in one of the two independent butyl groups at 200 K not seen at 100 K. The structure at 273 K (**II**), however, differed significantly, with large changes in the unit cell parameters from **Ib** to **II** ($\Delta a/\sigma = -172$, $\Delta b/\sigma = +330$, $\Delta c/\sigma = +236$) and conformational changes and additional disorder appearing for both butyl groups.

A primary structural feature found in all three structures is the orientation of the butyl groups towards each other in a columnar arrangement along the a axis (see Fig. 4) with hydrogen bonding between the ions on the “exterior” of the columns. This type of segregation is a common feature found in many ionic liquid crystal structures [4] that for longer chain ($n = 12-18$) 1-alkyl-3-methylimidazolium-based ionic liquids results in a bilayer structure. The range of hydrogen bonding interactions is similar to those found in the closely-related $[\text{C}_2\text{mim}][\text{NO}_3]$ [6, 53], but there is no

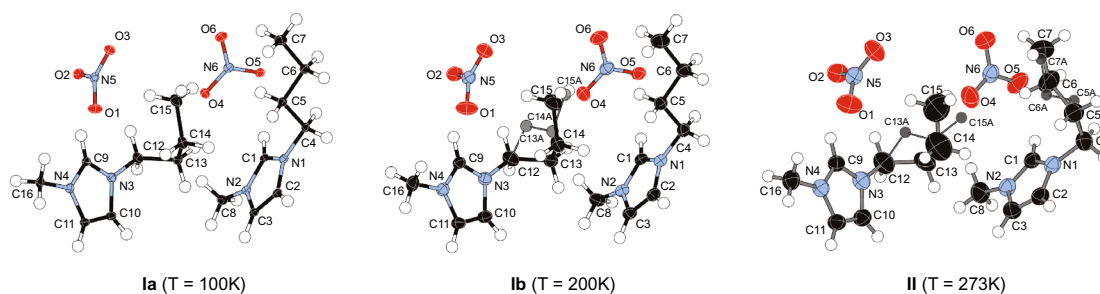


Fig. 3 Displacement ellipsoid diagrams of **Ia**, **Ib** and **II**. Disordered carbon atoms drawn as gray spheres without attached hydrogen atoms. Ellipsoids are drawn at the 50% level (Color figure online)

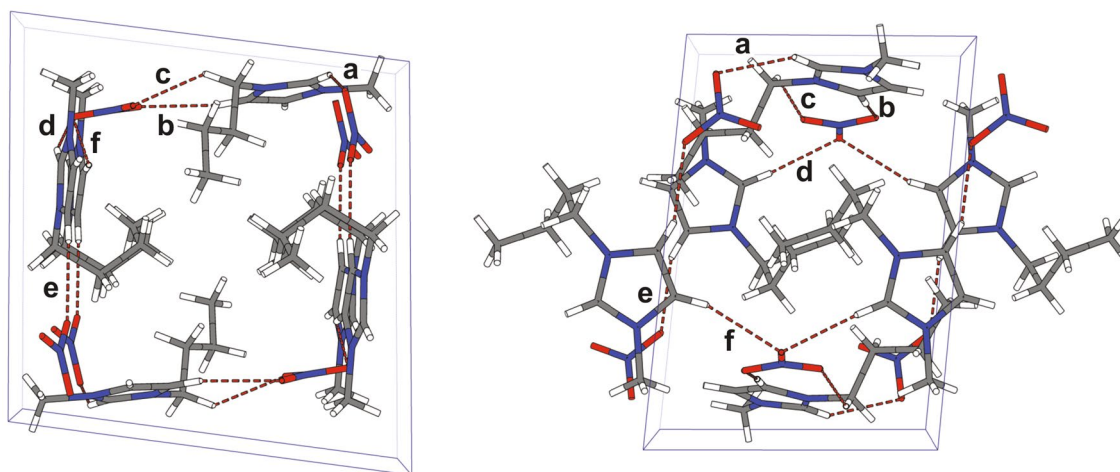


Fig. 4 Hydrogen bonding interactions (dashed red lines) in **Ia** viewed along the *a* axis (left) and *c* axis (right). Labels correspond to column one of Table 2 (Color figure online)

evidence of the $\pi\cdots\pi$ interactions seen in $[\text{C}_2\text{mim}][\text{NO}_3]$. There are interactions between the imidazolium ring and the nitrate ions [$d(\text{Cg}\cdots\text{N}) = 3.44\text{\AA}$] similar to those found in $[\text{C}_2\text{mim}][\text{NO}_3]$ [6].

Hydrogen bonding plays a significant role in the structure and properties of ionic liquids [54–56]. Analysis of the hydrogen bonding interactions in **Ia** and **Ib** (Tables 2 and 3) show a number of weak C–H \cdots O interactions. At lower temperature (100 K and 200 K) there are three C–H \cdots O contacts between each $[\text{C}_4\text{mim}]^+$ cation and the nitrate ions, as illustrated in Fig. 4. Most of the C–H \cdots O contacts are from the carbon atoms in the 2 and 5 ring positions (C1, C2, C9, C10, labeled as contacts (a), (b), (d), and (e), respectively), but the alpha carbon (C4) of the butyl group on one cation also forms a weak interaction (labeled as (c)). Similar hydrogen-bonding interactions are seen in other ionic liquids with oxyanions [7, 25].

The hydrogen bonding extends to form chains: C9–H9 \cdots O2 \cdots H11–C11, but only in the *a* direction. The interactions observed at 200 K (**Ib**) are very similar to those seen at 100 K (**Ia**) apart from a slight lengthening of the C–H \cdots O interactions (see Table 3 and Fig. 5). As illustrated in Fig. 5 and listed in Tables 2, 3, and 4, at 273 K (**II**) three of the six C–H \cdots O contacts are broken or significantly

Table 2 Hydrogen-bond distances and angles for **Ia**

	D–H \cdots A	D–H	H \cdots A	D \cdots A	D–H \cdots A
(a)	C1–H1 \cdots O5	0.95	2.32	3.1308 (14)	143
(b)	C2–H2 \cdots O3 ⁱ	0.95	2.36	3.3027 (14)	170
(c)	C4–H4B \cdots O1 ⁱ	0.99	2.42	3.2215 (15)	138
(d)	C9–H9 \cdots O2	0.95	2.33	3.2455 (15)	161
(e)	C10–H10 \cdots O6 ⁱⁱ	0.95	2.27	3.1637 (15)	157
(f)	C11–H11 \cdots O3 ⁱⁱ	0.95	2.53	3.2610 (15)	134

Symmetry codes: ⁱ $x - 1, y, z$; ⁱⁱ $-x + 1, -y + 1, -z + 1$

Table 3 Hydrogen-bond distances and angles for **Ib**

	D–H...A	D–H	H...A	D...A	D–H...A
(a)	C1–H1...O5	0.95	2.34	3.1649 (19)	145
(b)	C2–H2...O3	0.95	2.40	3.332 (2)	168
(c)	C4–H4A...O1	0.99	2.42	3.263 (2)	143
(d)	C9–H9...O2	0.95	2.36	3.265 (2)	160
(e)	C10–H10...O6 ⁱ	0.95	2.29	3.186 (2)	158
(f)	C11–H11...O3 ⁱⁱ	0.95	2.55	3.296 (2)	135

Symmetry codes: ⁱ $-x, -y + 1, -z + 1$; ⁱⁱ $x - 1, y, z$ **Table 4** Hydrogen-bond distances and angles for **II**

	D–H...A	D–H	H...A	D...A	D–H...A
(a)	C1–H1...O5 ⁱ	0.93	2.34	3.190 (3)	152
(c)	C4–H4BD...O1	0.97	2.36	3.298 (3)	162
(d)	C9–H9...O2	0.93	2.40	3.268 (3)	156
(e)	C10–H10...O6 ⁱⁱ	0.93	2.49	3.302 (3)	146
(g)	C13–H13B...O6 ⁱⁱ	0.97	2.47	3.337 (6)	149

Symmetry codes: ⁱ $-x + 1, -y + 1, -z + 1$; ⁱⁱ $-x, -y + 1, -z + 1$

weakened resulting in a loss of the (b) and (f) C–H...O contacts (see Fig. 6) and formation of a new C–H...O contact labeled as (g).

It is interesting to compare the structures obtained to those modeled by Cao, et al. [30] for the molecular dynamics simulations of a series of $[C_n\text{mim}][\text{NO}_3]$ ionic liquids ($n = 4\text{--}12$). They used the bilayer structure found for other long-chain $[C_n\text{mim}]^+$ salts with alkyl chains in the all-*trans* conformation as a starting point. For $[C_4\text{mim}][\text{NO}_3]$ they found that a pair of chains “take the gauche configuration” after equilibration. It is not clear from the text or figures

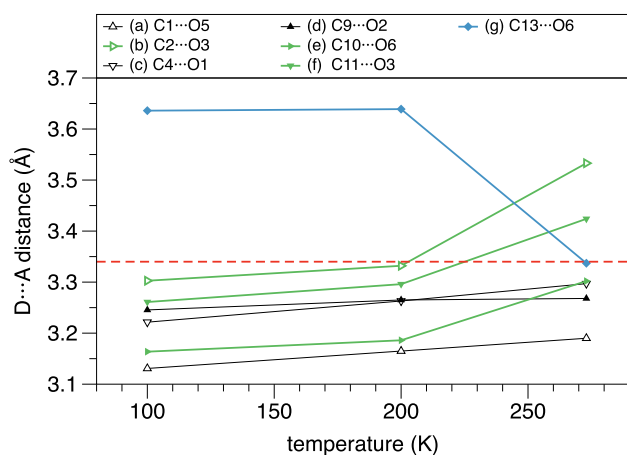


Fig. 5 Donor-acceptor distances (Å) found in each of the three structures, plotted versus temperature (K). Distances with large changes between 200 and 273 K are shown in green (increase) or blue (decrease). The dashed red line represents the donor-acceptor distance criterion used for tabulating contacts (3.34 Å) (Color figure online)

whether this refers to a GG, TG, or GT conformation. The derived unit cell parameters do not agree with the actual values for structure **Ib** (200 K), but the cell volume matches exactly within experimental error (1057 \AA^3). In their combined DSC/X-ray analysis, Abe et al. indexed the low-temperature form as monoclinic ($\beta = 95.35^\circ$) and the second (higher-temperature) form as orthorhombic and obtain a value of 8 for Z, none of which is consistent with our data. And comparison of the unit cell parameters for **Ia**, **Ib** and **II** to those obtained from powder diffraction experiments [33] also shows a lack of agreement.

Another useful comparison can be found between the molecular dynamics simulations of $[C_n\text{mim}][\text{NO}_3]$ [30] and the three structures determined in this report. From their simulations, Cao et al. describe the melting process as consisting of a transition to a metastable state where the polar and non-polar portions do not melt simultaneously. Rather they observe disorder in the alkyl side chains while the charged portions remain ordered. This description closely matches what we observe as the differences between the structures at 200 K (**Ib**) and 273 K (**II**).

Conformational Analysis

The imidazolium butyl chain conformations observed for all three structures are summarized in Table 5. At 100 K (Form **Ia**), one butyl group is in the lowest-energy TT [18, 32] conformation while the other is in the less common (and higher energy) G'G' conformation. At a temperature of 200 K (Form **Ib**), the butyl chain of the first cation remains ordered in the TT conformation, while the butyl chain of the second imidazolium is disordered with 87.6(4)% in the G'G' conformation and 12.4(4)% in the lower energy [32] GT conformation.

In the structure of Form **II**, determined at 273 K, both butyl chains are disordered, with complete loss of the TT conformation resulting in one chain distributed between G'T [56.9(6)%] and GT [43.1(6)%], and the second between G'G' [56.9(6)%] and GT [43.1(6)%]. The two disordered chains were initially modeled with independent occupancies and refined to the same value (within error). Inspection of a spacefilling model showed spatial clashes between the two butyl chains thus requiring that the conformations and occupancies of the two chains be correlated. The model was then modified to include a single free variable for the disorder of both butyl groups.

A search of the Cambridge Structural Database (CSD) for 1-butyl-3-methylimidazolium salts resulted in 225 hits representing 192 compounds, with some duplication and several examples of polymorphism [8, 11, 18, 28]. Of the 415 individual $[C_4\text{mim}]^+$ ions, seventy eight (19%) were modeled as disordered ions. The reported disorder frequency is likely an underestimate, however, as the displacement ellipsoids

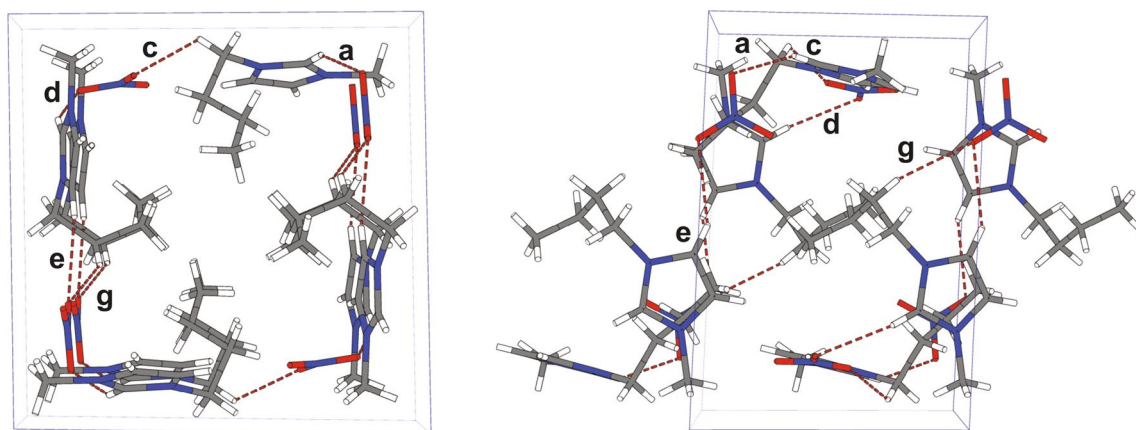


Fig. 6 Hydrogen bonding interactions (dashed red lines) in **II** viewed along the *a* axis (left) and the *c* axis (right). Labels correspond to column one of Table 4. Note the loss of C–H...O contacts (b) and (f) and the gain of (g) relative to **Ia** and **Ib** (Color figure online)

Table 5 Torsion angles and respective conformation labels for the 1-butyl-3-methylimidazolium ions in **Ia**, **Ib**, and **II**. See Fig. 1 for torsion angle (θ) and conformation label definitions

Structure	T (K)	Ion Pair	Occupancy	θ_1	θ_2	Conf. Label
Ia	100	1	1.000	−178.05 (9)	171.3 (1)	TT
Ia	100	2	1.000	−61.0 (1)	−64.5 (2)	G'G'
Ib	200	1	1.000	176.7 (1)	−172.4 (2)	TT
Ib	200	2	0.876 (4)	−60.7 (3)	−67.0 (4)	G'G'
Ib	200	2	0.124 (4)	67 (1)	−175 (2)	GT
II	273	1	0.569 (6)	−70.9 (5)	−166.6 (7)	G'T
II	273	1	0.431 (6)	70.0 (6)	167 (1)	GT
II	273	2	0.569 (6)	51.6 (9)	73 (1)	G'G'
II	273	2	0.431 (6)	−59.0 (8)	−161 (1)	GT

of many structures show evidence of unmodeled disorder as well as numerous entries containing whole-molecule disorder or where the cation electron density was modeled using SQUEEZE [57] (those structures were not included in this analysis). A histogram showing the relative abundance of ten common butyl chain conformations for the 225 hits found in the CSD is shown in Fig. 7. The distribution follows closely with the relative energy [32] of each conformation, with the TT, G'T and GT conformations found for nearly seventy percent of all ions.

A summary of crystallographic data and butyl conformations of $[\text{C}_4\text{mim}]^+$ salts with metal-free anions is shown in Table 6. This collection demonstrates a greater preference for the G'T and GT conformations (>60%) and less for the TT conformation (22%) than the overall analysis and energetics would predict. This could be due in part to the limited space available when the C_4mim^+ cation packs with smaller ions. The G'G' conformation found in $[\text{C}_4\text{mim}][\text{NO}_3]$ is quite uncommon (1.3% overall) and has not been seen previously in any of the small-ion $[\text{C}_4\text{mim}]^+$ structures.

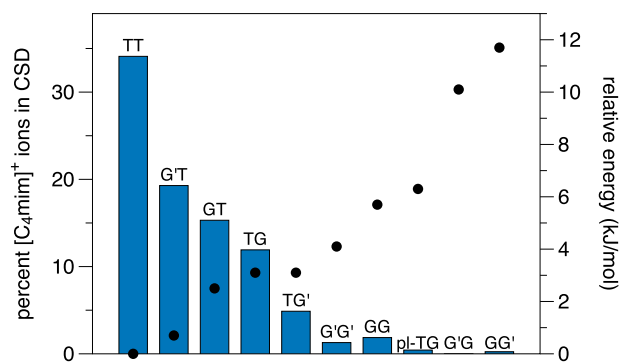


Fig. 7 Relative abundance and relative energy (kJ/mol) of ten common butyl chain configurations for 225 structures in the CSD (Color figure online)

Raman Spectroscopy

Raman spectra were collected on a sample of $[\text{C}_4\text{mim}][\text{NO}_3]$ at a range of temperatures and are shown in Fig. 8. Most of the major peaks in the 100 K spectrum can be assigned

Table 6 Summary of crystallographic details and conformations for selected metal-free 1-butyl-3-methylimidazolium salt structures

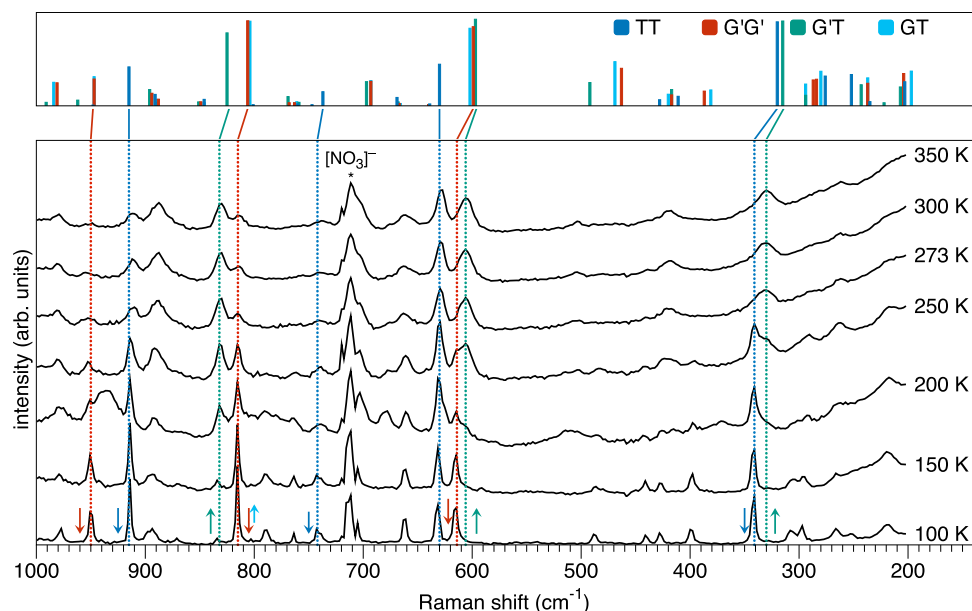
Anion	T (K)	Space group	Z'	Disorder	CSD refcode	Conformation 1	Conformation 2	Citation
NO ₃ ⁻	100	<i>P</i> $\bar{1}$	2	No		TT	G'G'	This work
NO ₃ ⁻	200	<i>P</i> $\bar{1}$	2	Yes		TT	G'G' (0.88)/GT	This work
NO ₃ ⁻	273	<i>P</i> $\bar{1}$	2	Yes		GT (0.57)/GT	G'G' (0.57)/GT	This work
F ⁻ ·H ₂ O	173	<i>P</i> 2 ₁ 2 ₁ 2 ₁	1	No	NAZHUS	GT		[9]
F ⁻ ·H ₂ O	199	<i>P</i> 2 ₁ 2 ₁ 2 ₁	1	No	NAZHUS01	GT		[10]
Cl ⁻	173	<i>P</i> 2 ₁ / <i>c</i>	1	No	TAJCUD	TT		[11]
Cl ⁻	173	<i>Pna</i> 2 ₁	1	No	TAJCUD01	GT		[11]
Cl ⁻	293	<i>P</i> 2 ₁ / <i>n</i>	1	No	TAJCUD02	TT		[12]
Cl ⁻	150	<i>P</i> 2 ₁ / <i>c</i>	1	No	TAJCUD03	TT		[13]
Cl ⁻	150	<i>Pna</i> 2 ₁	1	No	TAJCUD04	GT		[14]
Br ⁻	173	<i>Pna</i> 2 ₁	1	No	TAJDAK	GT		[11]
Br ⁻	293	<i>Pna</i> 2 ₁	1	No	TAJDAK01	GT		[15]
Br ⁻	110	<i>Pna</i> 2 ₁	1	No	TAJDAK02	GT		[16]
I ⁻	93	<i>P</i> 2 ₁ 2 ₁ 2 ₁	1	No	KETMAY	GT		[58]
PF ₆ ⁻	173	<i>P</i> $\bar{1}$	1	No	MAZXOB	GT		[17]
PF ₆ ⁻	183	<i>P</i> $\bar{1}$	1	No	MAZXOB01	GT		[7]
PF ₆ ⁻	100	<i>Pbca</i> (alpha)	1	No	MAZXOB02	GT		[18]
PF ₆ ⁻	193	<i>Pbca</i> (alpha)	1	Yes	MAZXOB03	GT (0.75)/G'T		[18]
PF ₆ ⁻	193	<i>P</i> $\bar{1}$ (beta)	2	Yes	MAZXOB04	TT	TG' (0.68)/TE'	[18]
PF ₆ ⁻	293	<i>P</i> $\bar{1}$ (beta)	2	Yes	MAZXOB05	TT (0.70)/TE'	TT (0.70)/TE'	[18]
PF ₆ ⁻	263	<i>P</i> $\bar{1}$ (gamma)	1	Yes	MAZXOB06	GT (0.92)/GT		[18]
Tf ₂ N ⁻	120	<i>P</i> 2 ₁ / <i>n</i>	2	Yes	IGUPUW	GT	G'T (0.70)/GT	[24]
BPh ₄ ⁻	173	<i>P</i> 2 ₁ 2 ₁ 2 ₁	1	No	WITJUE	GT		[19]
BPh ₄ ⁻	173	<i>P</i> 2 ₁ 2 ₁ 2 ₁	1	Yes	WITJUE01	GT (0.82)/G'T		[20]
B(p-tol) ₄ ⁻	110	<i>P</i> 2 ₁ / <i>c</i>	1	Yes	IKAQUG	GG (0.73)/GT		[21]
B(CF ₃ Ar) ₄ ⁻	110	<i>P</i> 2 ₁ / <i>c</i>	1	No	IKARAN	GT		[21]
BARF ⁻	200	<i>P</i> 2 ₁ / <i>n</i>	2	Yes	TAHMAR	TG' (0.75)/ET	TT (0.50)/TG	[22]
B(C ₆ F ₁₃ Ar) ₄ ⁻	150	<i>P</i> 4 ₁	1	No	IKARER	TT		[21]
B(C ₆ F ₅) ₄ ⁻	123	<i>P</i> 2 ₁ / <i>c</i>	1	No	PENREH	GT		[23]
HS ⁻	100	<i>Pna</i> 2 ₁	1	No	EKIBEH	GT		[27]
C ₂ O ₄ ²⁻	173	<i>P</i> 2 ₁ / <i>c</i>	1	Yes	DAZJIA	TT	G'T (0.92)/GT	[26]
<i>p</i> -tolSO ₃ ⁻	120	<i>P</i> $\bar{1}$	2	Yes	MIKYEL	TG	G'T (0.60)/GT	[16]
CF ₃ SO ₃ ⁻	200	<i>P</i> 2 ₁ / <i>n</i>	2	No	LAZRUA	GT	G'T	[7]
CH ₃ SO ₃ ⁻	173	<i>P</i> $\bar{1}$	1	No	VIGLUT	GT		[25]
CH ₃ OSO ₃ ⁻	173	<i>P</i> 2 ₁ / <i>c</i>	1	No	VIGMAA	GT		[25]

based on the structure **1a** and its TT and G'G' conformations. The strongest bands assignable to the TT conformation are found at 914, 742, 631 and 341 wavenumbers. These correlate well with data presented in previous work [39, 41] identifying characteristic bands for the TT conformer. All of these bands except the 631 cm⁻¹ band can be seen to significantly decrease in intensity as the temperature is increased, consistent with the crystallographic results. The lack of a corresponding change in intensity of the 631 cm⁻¹ band is puzzling, though the TT conformation might be expected to be present in samples at 300 K and above that are in the liquid state. A similar decrease in intensity of the peaks at

950, 815 and 615 cm⁻¹ assigned to the GG' conformation is observed in this set of data.

Additional peaks assignable to the G'T and GT conformations are also marked in Fig. 8. In some cases these peaks are coincident or nearly coincident with other peaks and thus may be difficult to distinguish. However, there is a clear increase in the peak at 330 cm⁻¹ that can be assigned to the G'T conformation that becomes particularly apparent at about 250 K. The liquid form (at 350 K) appears to contain significant amounts of the TT and G'T conformers, though this is not a comprehensive analysis and other conformers are likely to be present.

Fig. 8 Raman spectra collected on a sample of $[C_4mim][NO_3]$ at temperatures ranging from 100 to 350 K. DFT calculated bands for four conformers shown on top and highlighting significant peaks. Note: linear baseline correction applied to remove fluorescence background (Color figure online)



Conclusion

We have determined the crystal structures of two polymorphs (Form I and Form II) of 1-butyl-3-methylimidazolium nitrate at three temperatures (**Ia** at 100 K, **Ib** at 200 K and **II** at 273 K) showing changes in side-chain conformation and disorder as a function of temperature. Raman spectra at multiple temperatures confirm the presence of several butyl chain conformers and display changes consistent with the crystallographic models. Analysis of short contacts shows numerous hydrogen bonding interactions between cation C–H's and nitrate ion oxygen atoms. This well-characterized system displaying a solid-solid phase transition can serve as a model for future studies of phase changes and melting in imidazolium-based ionic liquids.

Funding This work was supported in part by the National Science Foundation through Grant No. CHE-0942850.

Data Availability Crystallographic data has been deposited with the CCDC and can be obtained free of charge via <http://www.ccdc.cam.ac.uk/structures>, or from the Cambridge Crystallographic Data Centre, 12 Union Road, Cambridge CB2 1EZ, UK; fax: (+44) 1223-336-033; or e-mail: deposit@ccdc.cam.ac.uk.

Code Availability Python code for the conformational analysis of 1-butyl-3-methylimidazolium ions using the CSD Python API is freely available at <https://gitlab.com/djohnston66/bmim-analysis>.

Declarations

Conflict of interest The authors declare no conflicts of interest or competing interests.

References

1. Welton T (1999) Room-temperature ionic liquids. Solvents for synthesis and catalysis. *Chem Rev* 99(8):2071–2084. <https://doi.org/10.1021/cr980032t>
2. Hallett JP, Welton T (2011) Room-temperature ionic liquids: solvents for synthesis and catalysis. 2. *Chem Rev* 111(5):3508–3576. <https://doi.org/10.1021/cr1003248>
3. Fedorov MV, Kornyshev AA (2014) Ionic liquids at electrified interfaces. *Chem Rev* 114(5):2978–3036. <https://doi.org/10.1021/cr400374x>
4. Hayes R, Warr GG, Atkin R (2015) Structure and nanostructure in ionic liquids. *Chem Rev* 115(13):6357–6426. <https://doi.org/10.1021/cr500411q>
5. Dean PM, Pringle JM, MacFarlane DR (2010) Structural analysis of low melting organic salts: perspectives on ionic liquids. *Phys Chem Chem Phys* 12(32):9144–9153. <https://doi.org/10.1039/C003519J>
6. Beichel W, Preiss UP, Benkml B, Steinfeld G, Eiden P, Kraft A, Krossing I (2013) Temperature dependent crystal structure analyses and ion volume determinations of organic salts. *Z Anorg Allg Chem* 639(12–13):2153–2161. <https://doi.org/10.1002/zaac.201300246>
7. Choudhury AR, Winterton N, Steiner A, Cooper AI, Johnson KA (2005) In situ crystallization of low-melting ionic liquids. *J Am Chem Soc* 127(48):16792–16793. <https://doi.org/10.1021/ja055956u>
8. Abe H, Kishimura H, Takekiyo T, Hanasaki T, Yoshimura Y, Hamaya N (2020) Low-temperature and high-pressure phase changes of room-temperature ionic liquids. *J Mol Liq* 300:112340. <https://doi.org/10.1016/j.molliq.2019.112340>
9. Swatloski RP, Holbrey JD, Rogers RD (2003) Ionic liquids are not always green: hydrolysis of 1-butyl-3-methylimidazolium hexafluorophosphate. *Green Chem* 5(4):361–363. <https://doi.org/10.1039/B304400A>
10. Bouvet S, Pégot B, Marrot J, Magnier E (2014) Solvent free nucleophilic introduction of fluorine with [bmim][F]. *Tetrahedron Lett* 55(4):826–829. <https://doi.org/10.1016/j.tetlet.2013.12.020>

- Holbrey JD, Reichert WM, Nieuwenhuyzen M, Johnson S, Seddon KR, Rogers RD (2003) Crystal polymorphism in 1-butyl-3-methylimidazolium halides: supporting ionic liquid formation by inhibition of crystallization. *Chem Commun* 14:1636. <https://doi.org/10.1039/B304543A>
- Saha S, Hayashi S, Kobayashi A, Hamaguchi H-O (2003) Crystal structure of 1-Butyl-3-methylimidazolium Chloride. A clue to the elucidation of the ionic liquid structure. *Chem Lett* 32(8):740–741. <https://doi.org/10.1246/cl.2003.740>
- Kärkkäinen J, Asikkala J, Laitinen RS, Lajunen MK (2004) Effect of temperature on the purity of product in the preparation of 1-butyl-3-methylimidazolium-based ionic liquids. *Z Naturforsch B* 59(7):763–770. <https://doi.org/10.1515/znB-2004-0704>
- Pulham C, Pringle J, Parkin A, Parsons S, Messenger D (2005) CSD Communication. <https://doi.org/10.5517/CC992J5>
- Ozawa R, Hayashi S, Saha S, Kobayashi A, Hamaguchi H-O (2003) Rotational isomerism and structure of the 1-butyl-3-methylimidazolium cation in the ionic liquid state. *Chem Lett* 32(10):948–949. <https://doi.org/10.1246/cl.2003.948>
- Vygodskii YS, Mel'nik OA, Lozinskaya EI, Shaplov AS, Malyshkina IA, Gavrilova ND, Lyssenko KA, Antipin MY, Golovanov DG, Korlyukov AA, Ignat'ev N, Welz-Biermann U (2007) The influence of ionic liquid's nature on free radical polymerization of vinyl monomers and ionic conductivity of the obtained polymeric materials. *Polym Adv Technol* 18(1):50–63. <https://doi.org/10.1002/pat.795>
- Dibrov SM, Kochi JK (2006) Crystallographic view of fluidic structures for room-temperature ionic liquids: 1-butyl-3-methylimidazolium hexafluorophosphate. *Acta Crystallogr C* 62(1):o19–o21. <https://doi.org/10.1107/S0108270105037200>
- Saouane S, Norman SE, Hardacre C, Fabbiani FPA (2013) Pinning down the solid-state polymorphism of the ionic liquid [bmim][PF6]. *Chem Sci* 4(3):1270. <https://doi.org/10.1039/C2SC21959J>
- Dupont J, Suarez PAZ, De Souza RF, Burrow RA, Kintzinger J-P (2000) CH- π interactions in 1-n-butyl-3-methylimidazolium tetraphenylborate molten salt: solid and solution structures. *Chem Eur J* 6(13):2377–2381. [https://doi.org/10.1002/1521-3765\(20000703\)6:13%3C2377::AID-CHEM2377%3E3.0.CO;2-L](https://doi.org/10.1002/1521-3765(20000703)6:13%3C2377::AID-CHEM2377%3E3.0.CO;2-L)
- Stenzel O, Raubenheimer HG, Esterhuysen C (2002) Biphasic hydroformylation in new molten salts—analogs and differences to organic solvents. *J Chem Soc Dalton Trans* 6:1132. <https://doi.org/10.1039/B107720A>
- van den Broeke J, Stam M, Lutz M, Kooijman H, Spek AL, Deelman B-J, van Koten G (2003) Designing ionic liquids: 1-butyl-3-methylimidazolium cations with substituted tetraphenylborate counterions. *Eur J Inorg Chem* 2003(15):2798–2811. <https://doi.org/10.1002/ejic.200300057>
- Finden J, Beck G, Lantz A, Walsh R, Zaworotko MJ, Singer RD (2003) Preparation and characterization of 1-butyl-3-methylimidazolium tetrakis(3,5-bis(trifluoromethyl) phenyl)borate, [bmim]BARF. *J Chem Crystallogr* 33(4):287–295. <https://doi.org/10.1023/A:1023885212233>
- Zhang B, Köberl M, Pöthig A, Cokoja M, Herrmann WA, Kühn FE (2012) Synthesis and characterization of imidazolium salts with the weakly coordinating [B(C6F5)4]⁻ anion. *Z Naturforsch B* 67(10):1030–1036. <https://doi.org/10.5560/znB.2012-0180>
- Paulechka YU, Kabo GJ, Blokhin AV, Shaplov AS, Lozinskaya EI, Golovanov DG, Lyssenko KA, Korlyukov AA, Vygodskii YS (2009) IR and X-ray Study of Polymorphism in 1-Alkyl-3-methylimidazolium Bis(trifluoromethanesulfonyl)imides. *J Phys Chem B* 113(28):9538–9546. <https://doi.org/10.1021/jp903702c>
- Santos CS, Rivera-Rubero S, Dibrov S, Baldelli S (2007) Ions at the surface of a room-temperature ionic liquid. *J Phys Chem C* 111(21):7682–7691. <https://doi.org/10.1021/jp0652751>
- Kuzmina O, Hassan NH, White AJ, Welton T (2017) CSD Communication. <https://doi.org/10.5517/ccdc.csd.cc1p2p1h>
- Finger LH, Sundermeyer J (2016) Halide-free synthesis of hydrochalcogenide ionic liquids of the type [cation][HE] (E=S, Se, Te). *Chem Eur J* 22(12):4218–4230. <https://doi.org/10.1002/chem.201504577>
- Hayashi S, Ozawa R, Hamaguchi H-O (2003) Raman spectra, crystal polymorphism, and structure of a prototype ionic-liquid [bmim]Cl. *Chem Lett* 32(6):498–499. <https://doi.org/10.1246/cl.2003.498>
- Endo T, Nishikawa K (2013) Thermal phase behavior of 1-butyl-3-methylimidazolium hexafluorophosphate: simultaneous measurements of the melting of two polymorphic crystals by Raman spectroscopy and calorimetry. *Chem Phys Lett* 584:79–82. <https://doi.org/10.1016/j.cplett.2013.08.052>
- Cao W, Wang Y, Saielli G (2018) Metastable state during melting and solid-solid phase transition of [CnMim][NO₃] (n = 4–12) ionic liquids by molecular dynamics simulation. *J Phys Chem B* 122(1):229–239. <https://doi.org/10.1021/acs.jpcc.7b09073>
- Strechan AA, Kabo AG, Paulechka YU, Blokhin AV, Kabo GJ, Shaplov AS, Lozinskaya EI (2008) Thermochemical properties of 1-butyl-3-methylimidazolium nitrate. *Thermochim Acta* 474(1):25–31. <https://doi.org/10.1016/j.tca.2008.05.002>
- Endo T, Hoshino S, Shimizu Y, Fujii K, Nishikawa K (2016) Comprehensive conformational and rotational analyses of the butyl group in cyclic cations: DFT calculations for imidazolium, pyridinium, pyrrolidinium, and piperidinium. *J Phys Chem B* 120(39):10336–10349. <https://doi.org/10.1021/acs.jpcc.6b07166>
- Abe H, Takekiyo T, Yoshimura Y, Saihara K, Shimizu A (2016) Anomalous freezing of nano-confined water in room-temperature ionic liquid 1-butyl-3-methylimidazolium nitrate. *ChemPhysChem* 17(8):1136–1142. <https://doi.org/10.1002/cphc.201501199>
- Talaty ER, Raja S, Storhaug VJ, Dölle A, Carper WR (2004) Raman and infrared spectra and ab initio calculations of C_{2–4} MIM imidazolium hexafluorophosphate ionic liquids. *J Phys Chem B* 108(35):13177–13184. <https://doi.org/10.1021/jp040199s>
- Berg RW, Deetlefs M, Seddon KR, Shim I, Thompson JM (2005) Raman and ab initio studies of simple and binary 1-alkyl-3-methylimidazolium ionic liquids. *J Phys Chem B* 109(40):19018–19025. <https://doi.org/10.1021/jp050691r>
- Heimer NE, Del Sesto RE, Meng Z, Wilkes JS, Carper WR (2006) Vibrational spectra of imidazolium tetrafluoroborate ionic liquids. *J Mol Liq* 124(1–3):84–95. <https://doi.org/10.1016/j.molliq.2005.08.004>
- Holomb R, Martinelli A, Albinsson I, Lassègues JC, Johansson P, Jacobsson P (2008) Ionic liquid structure: the conformational isomerism in 1-butyl-3-methylimidazolium tetrafluoroborate ([bmim][BF₄]). *J Raman Spectrosc* 39(7):793–805. <https://doi.org/10.1002/jrs.1912>
- Hamaguchi H-O, Ozawa R (2005) Structure of ionic liquids and ionic liquid compounds: are ionic liquids genuine liquids in the conventional sense? *Adv Chem Phys* 131:85–104
- Berg RW (2007) Raman spectroscopy and Ab-initio model calculations on ionic liquids. *Monatsh Chem* 138(11):1045–1075. <https://doi.org/10.1007/s00706-007-0760-9>
- Saha S, Hiroi T, Iwata K, Hamaguchi H-O (2015) Raman spectroscopy and the heterogeneous liquid structure in ionic liquids. In: Plechkova NV, Seddon KR (eds) *Ionic liquids completely uncoiled: critical expert overviews*. Wiley, Hoboken, pp 165–187
- Paschoal VH, Faria LFO, Ribeiro MCC (2017) Vibrational spectroscopy of ionic liquids. *Chem Rev* 117(10):7053–7112. <https://doi.org/10.1021/acs.chemrev.6b00461>
- Kausteklis J, Talaikis M, Aleksa V, Balevičius V (2018) Raman spectroscopy study of water confinement in ionic liquid

- 1-butyl-3-methylimidazolium nitrate. *J Mol Liq* 271:747–755. <https://doi.org/10.1016/j.molliq.2018.09.060>
43. Gruzdev MS, Ramenskaya LM, Chervonova UV, Kumeev RS (2009) Preparation of 1-butyl-3-methylimidazolium salts and study of their phase behavior and intramolecular interactions. *Russ J Gen Chem* 79(8):1720–1727. <https://doi.org/10.1134/S1070363209080246>
44. Solar M, Trapp N (2018) μ CHILL: a lightweight, modular system for handling crystalline samples at low temperatures under inert conditions. *J Appl Crystallogr* 51(2):541–548. <https://doi.org/10.1107/S1600576718003291>
45. Bruker (2019) APEX3, SAINT and SADABS. Bruker AXS Inc., Madison, WI
46. Sheldrick GM (2015) SHELXT—Integrated space-group and crystal-structure determination. *Acta Crystallogr A* 71(1):3–8. <https://doi.org/10.1107/S2053273314026370>
47. Sheldrick GM (2015) Crystal structure refinement with SHELXL. *Acta Crystallogr C* 71(1):3–8. <https://doi.org/10.1107/S2053229614024218>
48. Dolomanov OV, Bourhis LJ, Gildea RJ, Howard JAK, Puschmann H (2009) OLEX2: a complete structure solution, refinement and analysis program. *J Appl Crystallogr* 42(2):339–341. <https://doi.org/10.1107/S0021889808042726>
49. Palmer D (2020) CrystalMaker®: a crystal and molecular structures program for Mac and Windows. CrystalMaker Software Ltd, Oxford
50. Groom CR, Bruno IJ, Lightfoot MP, Ward SC (2016) The Cambridge structural database. *Acta Crystallogr B* 72(2):171–179. <https://doi.org/10.1107/S2052520616003954>
51. Daylight Chemical Information Systems (2019) SMARTS - A Language for Describing Molecular Patterns. <https://www.daylight.com/dayhtml/doc/theory/theory.smarts.html>
52. Spartan '18 (2018) Wavefunction, Inc., Irvine, CA
53. Wilkes JS, Zaworotko MJ (1992) Air and water stable 1-ethyl-3-methylimidazolium based ionic liquids. *J Chem Soc Chem Commun*. <https://doi.org/10.1039/C39920000965>
54. Tsuzuki S, Tokuda H, Mikami M (2007) Theoretical analysis of the hydrogen bond of imidazolium C₂-H with anions. *Phys Chem Chem Phys* 9(34):4780. <https://doi.org/10.1039/B707419K>
55. Fumino K, Wulf A, Ludwig R (2009) The potential role of hydrogen bonding in aprotic and protic ionic liquids. *Phys Chem Chem Phys* 11(39):8790. <https://doi.org/10.1039/B905634C>
56. Dong K, Zhang S, Wang J (2016) Understanding the hydrogen bonds in ionic liquids and their roles in properties and reactions. *Chem Commun* 52(41):6744–6764. <https://doi.org/10.1039/C5CC10120D>
57. Spek AL (2015) PLATON SQUEEZE: a tool for the calculation of the disordered solvent contribution to the calculated structure factors. *Acta Crystallogr C* 71(1):9–18. <https://doi.org/10.1107/S2053229614024929>
58. Nakakoshi M, Shiro M, Fujimoto T, Machinami T, Seki H, Tashiro M, Nishikawa K (2006) Crystal structure of 1-Butyl-3-methylimidazolium iodide. *Chem Lett* 35:1400–1401. <https://doi.org/10.1246/cl.2006.1400>

Authors and Affiliations

Dean H. Johnston¹  · Mallory Gasbarre¹ · Carolanne E. Norris¹

✉ Dean H. Johnston
djohnston@otterbein.edu

¹ Department of Chemistry, Otterbein University, Westerville, OH 43081, USA